

Measuring and imaging diffusion with multiple scan speed image correlation spectroscopy

Nadine Gröner,¹ Jérémie Capoulade,¹ Christoph Cremer,² and Malte Wachsmuth^{1,*}

¹Cell Biology & Biophysics Unit, European Molecular Biology Laboratory,
Meyerhofstraße 1, 69117 Heidelberg, Germany

²Applied Optics and Information Processing, Kirchhoff Institute of Physics, Ruprecht Karls University,
Im Neuenheimer Feld 227, 69120 Heidelberg, Germany

*malte.wachsmuth@embl.de

Abstract: The intracellular mobility of biomolecules is determined by transport and diffusion as well as molecular interactions and is crucial for many processes in living cells. Methods of fluorescence microscopy like confocal laser scanning microscopy (CLSM) can be used to characterize the intracellular distribution of fluorescently labeled biomolecules. Fluorescence correlation spectroscopy (FCS) is used to describe diffusion, transport and photo-physical processes quantitatively. As an alternative to FCS, spatially resolved measurements of mobilities can be implemented using a CLSM by utilizing the spatio-temporal information inscribed into the image by the scan process, referred to as raster image correlation spectroscopy (RICS). Here we present and discuss an extended approach, multiple scan speed image correlation spectroscopy (msICS), which benefits from the advantages of RICS, i.e. the use of widely available instrumentation and the extraction of spatially resolved mobility information, without the need of a priori knowledge of diffusion properties. In addition, msICS covers a broad dynamic range, generates correlation data comparable to FCS measurements, and allows to derive two-dimensional maps of diffusion coefficients. We show the applicability of msICS to fluorophores in solution and to free EGFP in living cells.

©2010 Optical Society of America

OCIS codes: (100.2960) Image analysis; (180.5810) Scanning microscopy; (300.6500) Spectroscopy, time-resolved.

References and links

1. E. L. Elson, and D. Magde, "Fluorescence correlation spectroscopy. I. Conceptual basis and theory," *Biopolymers* **13**(1), 1–27 (1974).
2. D. Magde, E. L. Elson, and W. W. Webb, "Fluorescence correlation spectroscopy. II. An experimental realization," *Biopolymers* **13**(1), 29–61 (1974).
3. D. A. Bulseco, D. E. Wolf, S. Greenfield, and E. W. David, "Fluorescence Correlation Spectroscopy: Molecular Complexing in Solution and in Living Cells," in *Digital Microscopy, 3rd Edition* (Academic Press, 2007), pp. 525–559.
4. D. Grünwald, M. C. Cardoso, H. Leonhardt, and V. Buschmann, "Diffusion and binding properties investigated by Fluorescence Correlation Spectroscopy (FCS)," *Curr. Pharm. Biotechnol.* **6**(5), 381–386 (2005).
5. M. Wachsmuth, and K. Weisshart, "Fluorescence photobleaching and fluorescence correlation spectroscopy: two complementary technologies to study molecular dynamics in living cells," in *Imaging Cellular and Molecular Biological Functions* (Springer Verlag, Heidelberg, 2007).
6. W. B. Amos, and J. G. White, "How the confocal laser scanning microscope entered biological research," *Biol. Cell* **95**(6), 335–342 (2003).
7. C. Cremer, and T. Cremer, "Considerations on a laser-scanning-microscope with high resolution and depth of field," *Microsc. Acta* **81**(1), 31–44 (1978).
8. J. Pawley, *Handbook of Biological Confocal Microscopy* (Springer, Berlin, 2006).
9. G. Rabut, J. Ellenberg, D. Spector, and D. Goldman, "Photobleaching Techniques to Study Mobility and Molecular Dynamics of Proteins in Live Cells: FRAP, iFRAP, and FLIP," in *Live Cell Imaging - A Laboratory Manual* (CSHL Press, Cold Spring Harbor, 2005), pp. 101–126.
10. M. E. van Royen, P. Farla, K. A. Mattern, B. Geverts, J. Trapman, and A. B. Houtsmuller, "Fluorescence recovery after photobleaching (FRAP) to study nuclear protein dynamics in living cells," *Methods Mol. Biol.* **464**, 363–385 (2009).

11. N. O. Petersen, P. L. Höddelius, P. W. Wiseman, O. Seger, and K. E. Magnusson, "Quantitation of membrane receptor distributions by image correlation spectroscopy: concept and application," *Biophys. J.* **65**(3), 1135–1146 (1993).
12. N. O. Petersen, R. Rigler, and E. S. Elson, "FCS and spatial correlations on biological surfaces," in *Fluorescence Correlation Spectroscopy - Theory and Applications* (Springer, Heidelberg, 2001), pp. 162–184.
13. D. L. Kolin, S. Costantino, and P. W. Wiseman, "Sampling effects, noise, and photobleaching in temporal image correlation spectroscopy," *Biophys. J.* **90**(2), 628–639 (2006).
14. D. L. Kolin, D. Ronis, and P. W. Wiseman, "k-Space image correlation spectroscopy: a method for accurate transport measurements independent of fluorophore photophysics," *Biophys. J.* **91**(8), 3061–3075 (2006).
15. D. L. Kolin, and P. W. Wiseman, "Advances in image correlation spectroscopy: measuring number densities, aggregation states, and dynamics of fluorescently labeled macromolecules in cells," *Cell Biochem. Biophys.* **49**(3), 141–164 (2007).
16. C. M. Brown, R. B. Dalal, B. Hebert, M. A. Digman, A. R. Horwitz, and E. Gratton, "Raster image correlation spectroscopy (RICS) for measuring fast protein dynamics and concentrations with a commercial laser scanning confocal microscope," *J. Microsc.* **229**(1), 78–91 (2008).
17. M. A. Digman, C. M. Brown, P. Sengupta, P. W. Wiseman, A. R. Horwitz, and E. Gratton, "Measuring fast dynamics in solutions and cells with a laser scanning microscope," *Biophys. J.* **89**(2), 1317–1327 (2005).
18. M. A. Digman, and E. Gratton, "Analysis of diffusion and binding in cells using the RICS approach," *Microsc. Res. Tech.* **72**(4), 323–332 (2009).
19. M. A. Digman, P. W. Wiseman, C. Choi, A. R. Horwitz, and E. Gratton, "Stoichiometry of molecular complexes at adhesions in living cells," *Proc. Natl. Acad. Sci. U.S.A.* **106**(7), 2170–2175 (2009).
20. E. Gielen, N. Smisdom, M. Vandeven, B. De Clercq, E. Gratton, M. Digman, J.-M. Rigo, J. Hofkens, Y. Engelborghs, and M. Ameloot, "Measuring Diffusion of Lipid-like Probes in Artificial and Natural Membranes by Raster Image Correlation Spectroscopy (RICS): Use of a Commercial Laser-Scanning Microscope with Analog Detection," *Langmuir* (2009).
21. M. A. Digman, R. Dalal, A. F. Horwitz, and E. Gratton, "Mapping the number of molecules and brightness in the laser scanning microscope," *Biophys. J.* **94**(6), 2320–2332 (2008).
22. V. Vukojević, M. Heidkamp, Y. Ming, B. Johansson, L. Terenius, and R. Rigler, "Quantitative single-molecule imaging by confocal laser scanning microscopy," *Proc. Natl. Acad. Sci. U.S.A.* **105**(47), 18176–18181 (2008).
23. K. M. Berland, P. T. C. So, Y. Chen, W. W. Mantulin, and E. Gratton, "Scanning two-photon fluctuation correlation spectroscopy: particle counting measurements for detection of molecular aggregation," *Biophys. J.* **71**(1), 410–420 (1996).
24. D. E. Koppel, F. Morgan, A. E. Cowan, and J. H. Carson, "Scanning concentration correlation spectroscopy using the confocal laser microscope," *Biophys. J.* **66**(2), 502–507 (1994).
25. J. Ries, S. Chiantia, and P. Schwille, "Accurate determination of membrane dynamics with line-scan FCS," *Biophys. J.* **96**(5), 1999–2008 (2009).
26. J. Widengren, Ü. Mets, and R. Rigler, "Fluorescence Correlation Spectroscopy of Triplet States in Solution: A Theoretical and Experimental Study," *J. Phys. Chem.* **99**(36), 13368–13379 (1995).
27. "LFD Workshop 2006 - Laboratory for Fluorescence Dynamics" (2006), <http://www.lfd.uci.edu/workshop/2006/>.
28. M. Wachsmuth, "Method for measuring fluorescence fluctuations in the presence of slow signal fluctuations," US Patent No. 7,154,602 (2006).
29. G. S. Harms, L. Cognet, P. H. Lommerse, G. A. Blab, and T. Schmidt, "Autofluorescent proteins in single-molecule research: applications to live cell imaging microscopy," *Biophys. J.* **80**, 2396–2408 (2001).
30. J. R. Lakowicz, *Principles of Fluorescence Spectroscopy* (Kluwer Academic/Plenum Publishers, New York, 1999).
31. M. Wachsmuth, W. Waldeck, and J. Langowski, "Anomalous diffusion of fluorescent probes inside living cell nuclei investigated by spatially-resolved fluorescence correlation spectroscopy," *J. Mol. Biol.* **298**(4), 677–689 (2000).
32. I. Gregor, D. Patra, and J. Enderlein, "Optical saturation in fluorescence correlation spectroscopy under continuous-wave and pulsed excitation," *ChemPhysChem* **6**(1), 164–170 (2005).
33. P. Dittrich, F. Malvezzi-Campeggi, M. Jahnz, and P. Schwille, "Accessing molecular dynamics in cells by fluorescence correlation spectroscopy," *Biol. Chem.* **382**(3), 491–494 (2001).
34. P. Schwille, U. Haupts, S. Maiti, and W. W. Webb, "Molecular dynamics in living cells observed by fluorescence correlation spectroscopy with one- and two-photon excitation," *Biophys. J.* **77**(4), 2251–2265 (1999).
35. K. P. Müller, F. Erdel, M. Caudron-Herger, C. Marth, B. D. Fodor, M. Richter, M. Scaranaro, J. Beaudouin, M. Wachsmuth, and K. Rippe, "Multiscale analysis of dynamics and interactions of heterochromatin protein 1 by fluorescence fluctuation microscopy," *Biophys. J.* **97**(11), 2876–2885 (2009).
36. J. Beaudouin, F. Mora-Bermúdez, T. Klee, N. Daigle, and J. Ellenberg, "Dissecting the contribution of diffusion and interactions to the mobility of nuclear proteins," *Biophys. J.* **90**(6), 1878–1894 (2006).
37. C. Pack, K. Saito, M. Tamura, and M. Kinjo, "Microenvironment and effect of energy depletion in the nucleus analyzed by mobility of multiple oligomeric EGFPs," *Biophys. J.* **91**(10), 3921–3936 (2006).
38. M. Wachsmuth, M. Caudron-Herger, and K. Rippe, "Genome organization: balancing stability and plasticity," *Biochim. Biophys. Acta* **1783**(11), 2061–2079 (2008).
39. N. Dross, C. Spriet, M. Zwerger, G. Müller, W. Waldeck, J. Langowski, and J. Z. Rappoport, "Mapping eGFP oligomer mobility in living cell nuclei," *PLoS ONE* **4**(4), e5041–e5041 (2009).

40. A. Bancaud, S. Huet, N. Daigle, J. Mozziconacci, J. Beaudouin, and J. Ellenberg, "Molecular crowding affects diffusion and binding of nuclear proteins in heterochromatin and reveals the fractal organization of chromatin," *EMBO J.* **28**(24), 3785–3798 (2009).
 41. C. M. Roth, P. I. Heinlein, M. Heilemann, and D.-P. Herten, "Imaging diffusion in living cells using time-correlated single-photon counting," *Anal. Chem.* **79**(19), 7340–7345 (2007).
 42. G. Heuvelman, F. Erdel, M. Wachsmuth, and K. Rippe, "Analysis of protein mobilities and interactions in living cells by multifocal fluorescence fluctuation microscopy," *Eur. Biophys. J.* **38**(6), 813–828 (2009).
 43. B. Kannan, L. Guo, T. Sudhaharan, S. Ahmed, I. Maruyama, and T. Wohland, "Spatially Resolved Total Internal Reflection Fluorescence Correlation Microscopy Using an Electron Multiplying Charge-Coupled Device Camera," *Analytical Chemistry* (2007).
 44. D. J. Needleman, Y. Xu, and T. J. Mitchison, "Pin-hole array correlation imaging: highly parallel fluorescence correlation spectroscopy," *Biophys. J.* **96**(12), 5050–5059 (2009).
-

1. Introduction

Since its inception in the 1970s [1, 2] fluorescence correlation spectroscopy (FCS) has emerged as a very useful method for probing transport, diffusion and interactions of biomolecules in vitro and in vivo [3–5]. It offers information at the single molecule level while it ensures good statistical relevance by averaging over the behavior of many molecules. FCS is based on a confocal laser illumination and fluorescence detection scheme providing a small diffraction-limited focus as observation volume. The detection of fluctuations in molecular concentrations and (bio-)chemical states within this volume allows to determine diffusion and interaction properties even in subcellular structures by computing the temporal autocorrelation function of the fluorescence signal emitted from within the focus. FCS covers a concentration range between ~100 pM and ~1 μ M and a time scale between nanoseconds and seconds.

Due to the suppression of scattered light and the diffraction-limited resolution in three dimensions, a confocal setup allows to probe the spatial distribution of fluorescent molecules by raster-scanning pixel by pixel and line by line the focus over the sample using rotary galvanometer-driven mirrors effectively located in the back focal plane of the objective lens [6–8]. This forms the foundation of confocal laser scanning microscopy (CLSM), a mode of fluorescence microscopy widely used in modern biology to visualize cells and cellular components.

A confocal image frame is usually assumed to be taken instantaneously, and time-resolved information is obtained from time series of images. For example, in an imaging-based fluorescence recovery after photobleaching (FRAP) experiment, an area of a cell is depleted of fluorescent molecules by photobleaching induced by high-intensity illumination [5, 9, 10]. Subsequently the redistribution of the remaining fluorescent molecules and the corresponding recovery of the fluorescence signal are observed over time. Moreover, in some image correlation spectroscopy (ICS) approaches [11, 12] the signal at each pixel is extracted from every frame to obtain intensity traces for every pixel comparable to FCS data [13–15], albeit with a time resolution well above 1 ms.

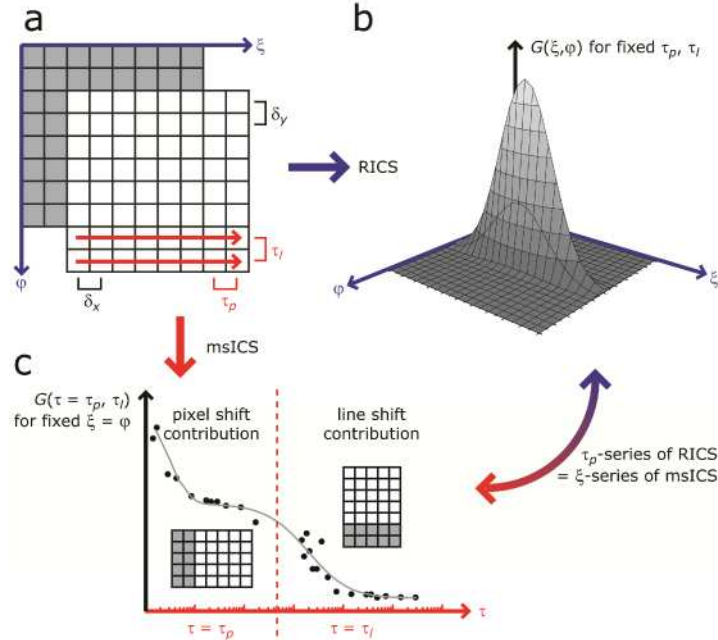


Fig. 1. Principle of RICS and msICS. (a) Confocal images scanned unidirectionally with well defined scanning velocity, pixel size, pixel dwell time and line scan time are subject to a two-dimensional spatial autocorrelation analysis. (b) For RICS, a two-dimensional autocorrelation function for a given scanning velocity is generated and fitted with a model function describing transport/diffusion, photophysical and interaction process to extract the spatio-temporal information inscribed into the image by the scanning process. (c) For msICS, a one-dimensional representation of the resulting autocorrelation function for a given pixel shift is generated as a function of the lag time given by the pixel dwell time for smaller and by the line time for larger times resulting from different scanning velocities and is fitted accordingly.

However, a CLSM image contains more information: due to the sequential nature of the scanning process the spatial and temporal division of the pixels, i.e. the sampling, is known since it is determined by the scanner settings. Typical pixel dwell times are in the range of μs , the time lags between lines in the range of ms and the times between successive images in the range of s. The spatial gap between pixels on the raster, the pixel shift, is in the range of a few 10 to several 100 nm. The well-defined spatio-temporal acquisition allows to assess diffusion and transport properties of the molecules similar to FCS by applying a spatial correlation analysis to the images, see Fig. 1. This forms the basis of raster image correlation spectroscopy (RICS [16, 17];), a recently introduced image correlation spectroscopy technique. RICS has been applied to diffusion and binding [18], e.g. to the detection of protein complexes [19] in living cells or the mobility of lipid-like probes in membranes [20]. It also allows to map diffusion and interaction properties and is related to other approaches that implement fluctuation spectroscopy techniques in an imaging context [21, 22].

Usually RICS is performed with fixed scanner settings resulting in pre-defined spatio-temporal sampling. However, it would be desirable to uncouple spatial and temporal sampling while retaining the major benefit of RICS, i.e. access to spatially resolved mobility information from confocal images. Moreover, without *a priori* knowledge of the time scale of the processes of interest it is sometimes difficult to adjust the sampling properly. Therefore we present here an extension of the concept of RICS to series of scanning velocities: several time series of the same sample are acquired, for which the pixel dwell time is varied whereas the other parameters are kept constant, corresponding to several RICS measurements and referred to in the following as multiple scan speed intensity correlation spectroscopy (msICS). The correlated image is computed in the same way as for RICS. However, instead of plotting the correlation function over the pixel shift for a fixed pixel dwell and line scan time, which is

determined by the pixel dwell time and the number of pixels per line, we use the different pixel dwell/line scan times to generate a temporal autocorrelation function for every pixel shift, see Fig. 1c. In order to create a correlation function over a broad time scale, the correlation values for the various pixel dwell times are taken for a fixed pixel shift along the line and combined with the correlation values for the various line scan times for the same pixel shift perpendicular to the line. In this way msICS covers a broad dynamic range and in particular for pixel shifts smaller than the diffraction limit, the resulting autocorrelation function resembles a point FCS measurement. When applied to subregions of the images, spatially resolved data can be obtained resulting in maps of correlation functions and of parameters derived thereof. In addition to the underlying concept we show here that msICS can be applied even to molecules as fast as fluorophores in solution and free EGFP expressed in HeLa cells.

2. Theory

2.1 Raster image correlation spectroscopy (RICS)

The theoretical foundation of RICS has been published previously [16, 17]. In order to access the dynamic information inscribed into a confocal image the spatial correlation function of an image is computed according to

$$G_{\text{RICS}}(\xi, \varphi) = \frac{\langle I(x, y)I(x + \xi, y + \varphi) \rangle}{\langle I(x, y) \rangle^2}. \quad (1)$$

This contains information about the probability that light detected at pixels (x, y) and $(x + \xi, y + \varphi)$ stems from the same molecule. The movement of the molecule is independent of the scanning process, thus the autocorrelation curve splits up into two parts: $G_{\text{RICS}} \propto G_D \times G_S$ is the product of the diffusion part G_D and the scanning part G_S .

Using the characteristic diffusion correlation time $\tau_{\text{diff}} = w_0^2 / 4D$, where w_0 is the $1/e^2$ radius of the focal volume or point spread function (PSF) of the optical system and D the diffusion coefficient, as well as the pixel dwell time τ_p and the line scan time τ_l in $\tau = \tau_p \xi + \tau_l \varphi$ and the pixel shift or size in the image $(\delta_x \times \delta_y)$ along (x) and perpendicular (y) to the line, we obtain [17, 23–25]:

$$G_{\text{RICS}} = \frac{1}{N} \overbrace{\left[1 + \frac{4D(\tau_p \xi + \tau_l \varphi)}{w_0^2} \right]^{-1} \left[1 + \frac{4D(\tau_p \xi + \tau_l \varphi)}{\kappa^2 w_0^2} \right]^{-1/2}}^{=G_D} \underbrace{\exp \left[-\frac{(\delta_x \xi / w_0)^2 + (\delta_y \varphi / w_0)^2}{1 + 4D(\tau_p \xi + \tau_l \varphi) / w_0^2} \right]}_{=G_S} \times \left[1 + \theta \exp \left(-\frac{\tau_p \xi + \tau_l \varphi}{\tau_{\text{trip}}} \right) \right] \quad (2)$$

with N being the average number of molecules in the focal volume. The last factor describes the occupation of the triplet state we have to consider with the triplet lifetime τ_{trip} and the fraction T of molecules being in the triplet state used in $\theta = T / (1 - T)$ [26].

2.2 Estimation of appropriate parameters

For a successful RICS experiment one has to choose appropriately the pixel size, the pixel dwell time and the number of pixels, which altogether determine the line scan time. These parameters are crucial for proper sampling of the diffusion process under investigation and difficult to specify especially when the magnitude of the diffusion coefficient is unknown.

There are two guidelines to meet this challenge: the pixel size should be 3- to 4-fold smaller than the PSF radius w_0 [17] and the pixel dwell time should be chosen according to the expected order of magnitude of the diffusion coefficient [27].

Alternatively, the range of appropriate parameters for a given diffusion coefficient can be estimated from diffusion theory: the probability to detect a particle in an isotropic and homogenous medium at (\mathbf{r}, t) that has resided earlier at $(\mathbf{r} = 0, t = 0)$ is given as

$$P(\mathbf{r}, t) = (4\pi Dt)^{-3/2} \exp\left(-\frac{\mathbf{r}^2}{4Dt}\right). \quad (3)$$

$P(\mathbf{r}_0, t)$ is maximal at t_0 , if

$$\left. \frac{\partial P}{\partial t} \right|_{t=t_0} = 0 \Leftrightarrow t_0 = \frac{r_0^2}{6D}. \quad (4)$$

In order to ensure distinct fluctuations as required for a significant correlation amplitude, $r_0 = w_0$ is set to allow particles to enter and leave the detection volume. The scan velocity $v = \delta_r / \tau_p$ should be close to $r_0 / t_0 = 6D / w_0$ (assuming square pixels with $\delta_r = \delta_x = \delta_y$). In addition, high spatial sampling, $\delta_r < w_0$, should be chosen to ensure that the laser beam can “follow” the particles even though due to oversampling immobile particles can be detected in several neighboring pixels.

2.3 Multiple scan speed image correlation spectroscopy (msICS)

To cover a broad dynamic range of diffusion properties we have developed an extended approach referred to as multiple scan speed image correlation spectroscopy (msICS): the idea is to measure several time series with varying pixel dwell times (achieved by changing the scanning velocity) and otherwise constant settings (corresponding to different RICS experiments). For statistical reasons we may take more than one frame for each pixel dwell time while keeping the total acquisition time for each scan velocity constant. We calculate the correlated image as defined above and as applied for RICS but instead of plotting and fitting the correlation function over the pixel shift (ξ, φ) in two dimensions we take a fixed pixel shift along the line $(\xi, 0)$ and plot the correlation values as a function of the pixel dwell time. In the same one-dimensional graph, we take the same pixel shift perpendicular to the line $(0, \xi)$ and plot the correlation values as a function of the line scan time. Since on the one hand the pixel dwell time and the line scan time usually differ by 2-3 orders of magnitude and on the other hand the pixel dwell times lie between $\sim 1 \mu\text{s}$ and $\sim 1 \text{ms}$, the resulting correlation function covers a broad time range between $\sim 1 \mu\text{s}$ and $\sim 1 \text{s}$ as shown in Fig. 1c.

Post data acquisition the shift parameter ξ can be chosen freely, rendering global fits possible. To obtain a comparable number of photons, image series are acquired for the same overall time for every scanning velocity. This results in different numbers of frames for each velocity because it takes longer to acquire a frame for a slow scanning velocity (and a long pixel dwell time) than for a fast scanning velocity (and a short pixel dwell time).

2.4 Correction for photobleaching and slowly mobile or immobile structures

Even when using highly sensitive photon counting detectors and very low laser intensities the acquisition of image series inevitably reduces the number of fluorescent molecules due to photobleaching. Any correlation spectroscopy approach is very sensitive to this because the correlation amplitude is inversely proportional to the concentration, see Eq. (2). Therefore we correct the calculated correlation matrix M_{corr} of each image or region of interest (ROI) i with

the respective mean intensity \bar{I}_i normalized to the mean intensity of the first image or ROI \bar{I}_0 :

$$M_{\text{corr},i}^{\text{new}} = \frac{\bar{I}_i}{\bar{I}_0} M_{\text{corr},i}^{\text{old}} \quad (5)$$

as suggested previously [16]. In addition, slowly mobile or immobile structures can result in a correlation overlaying the diffusional contribution. Therefore each ROI is first filtered with a moving average approach [25, 28] and then correlated: every pixel intensity value $v_p(x, y)$ is corrected with the difference between a local mean value $\bar{v}_{\text{local},d}(x, y)$ averaged over an array of $d \times d$ pixels centered around (x, y) and the mean value of the ROI \bar{v}_{global} according to

$$v_{p,i}^{\text{new}} = v_{p,i}^{\text{old}} - (\bar{v}_{\text{local},d} - \bar{v}_{\text{global}}). \quad (6)$$

The parameter d has to be optimized for every experiment and does not necessarily match the ROI size.

2.5 Fluorescence saturation

Taking into consideration the steps of excitation and emission as parts of the fluorescence process, it can be shown that the fluorescence yield F does not depend linearly on the excitation intensity I but obeys [29, 30,]:

$$F \propto \frac{I}{I + I_s} \quad (7)$$

where I_s is referred to as saturation intensity, i.e. the excitation intensity where the fluorescence yield reaches 50% of the maximum or saturation value.

3. Materials and methods

3.1 Mammalian cell culture and in vitro samples

For in vivo experiments, HeLa cells expressing free EGFP were seeded in 8 well Nunc LabTek chambered coverglasses (Thermo Fischer Scientific, Langensfeld, Germany) with phenol red-free RPMI medium. For in vitro experiments, Alexa488 (Invitrogen, Karlsruhe, Germany) and 150 kDa Dextran labelled with TRITC (Sigma Aldrich, Munich, Germany) were dispensed in 8 well LabTek chambered coverglasses, too, at the concentrations as given below.

3.2 Acquisition of CLSM and FCS data

Confocal fluorescence image series and FCS data were acquired on an inverted Leica confocal laser scanning microscope TCS SP5 AOBs SMD FCS equipped with an HCX Plan Apo CS 63 \times /1.2 NA water immersion objective lens (Leica Microsystems, Mannheim, Germany). For excitation, the 488 nm line of an Ar laser was used. The fluorescence was detected with an SPCM-AQR-14 avalanche photodiode (Perkin-Elmer Optoelectronics, Vaudreuil, Canada) behind a bandpass filter offering a transmission window of 500-550 nm. The diameter of the detection pinhole was set to the size of 1 Airy disk. The laser power in the sample was set to well below 200 μ W for FCS and below 500 μ W for CLSM acquisition. The laser power was measured in front of the objective lens using a Nova II power meter equipped with a PD300 detector (Ophir Optronics, Jerusalem, Israel). In vivo experiments were carried out at 37°C using an incubation chamber enclosing the microscope stage and body (EMBL workshops).

For image acquisition, the physical scanning velocity was determined by the scanning frequency f_{scan} of the galvanometer-driven x axis mirror given in lines per second (Hz), by the

zoom factor defining the physical length of the scanned line and by the number of pixels per line. Images were recorded with 16 bit resolution and stored in TIFF format using the LAS AF software of the microscope. With the detector gain the scaling factor between intensity values and photon counts could be changed. The image size was set to $N_x \times N_y = 1025 \times 512$ or 512×512 pixels and the pixel size δr to 30 nm. msICS experiments were performed with a scanning frequency of 500, 400, 200, 150, 100, 75, 50, 35, 20, 15, 10, and 5 Hz.

Due to the sinusoidal scanning process the pixel dwell time depends in principle on the pixel position. However, the duty cycle of the scanner, i.e. the amplitude fraction that is actually used for image formation, is 80% so that one can show that the variation of the pixel dwell time throughout the field of view is less than 10% when restricting the analysis to the central 50% of the image in horizontal direction, which was implemented for all experiments in this study. Therefore we set $\tau_l = 1/f_{\text{scan}}$ and $\tau_p \approx 0.258/(f_{\text{scan}} N_x)$.

For FCS data acquisition, the beam was parked at a position of interest, and laser illumination and detector read-out were started for typically 60 s. Data were acquired using the PicoQuant SymPhoTime software of the microscope and stored in binary raw format.

3.3 Processing and analysis of images for RICS/msICS and of FCS data

ImageJ (NIH, Bethesda, MD, USA) was used to view image series for RICS and msICS and to select ROIs if applicable. The whole data analysis workflow was developed and run in Matlab (The MathWorks, Natick, MA, USA) using the Image Processing Toolbox. After importing the image files as data matrices, ROIs could be selected. The slowly mobile/immobile background correction was applied according to Eq. (6). The image matrix was autocorrelated directly and weighted to correct for photobleaching as described before in Eq. (5). This was done separately for every taken image and an averaged correlation matrix was calculated. The whole process was repeated for every measured scanning frequency or pixel dwell time, respectively. Finally the desired representation of the data (RICS, msICS) was extracted and fitted with the model function Eq. (2).

FCS raw data were correlated with the Fluctuation Analyzer software written in our laboratory and fitted with Origin (OriginLab, Northampton, MA, USA) using the equation:

$$G(\tau) = \frac{1}{N} \left[f_1 \left[1 + \left(\frac{\tau}{\tau_{\text{diff},1}} \right)^{\alpha_1} \right]^{-1} \left[1 + \frac{1}{\kappa^2} \left(\frac{\tau}{\tau_{\text{diff},1}} \right)^{\alpha_1} \right]^{-1/2} + (1 - f_1) \left[1 + \left(\frac{\tau}{\tau_{\text{diff},2}} \right)^{\alpha_2} \right]^{-1} \left[1 + \frac{1}{\kappa^2} \left(\frac{\tau}{\tau_{\text{diff},2}} \right)^{\alpha_2} \right]^{-1/2} \right] \left[1 + \theta \exp \left(-\frac{\tau}{\tau_{\text{trip}}} \right) \right] \quad (8)$$

which describes two components featuring anomalous diffusion (characterized by τ_{diff} and the anomaly parameter α) and triplet occupation kinetics [31].

4. Results and discussion

4.1 Characterization of the PSF – saturation effects and the w_0 map

Saturation of the fluorophores can occur at sufficiently high laser power and affect the PSF by effectively increasing the focal radius [32]. This can result in an underestimation of the diffusion coefficient. In order to rule out saturation effects we have measured the mean fluorescence signal of confocal images of Alexa488 in aqueous solution (20 nM) as a function of the excitation laser power as shown in Fig. 2a. A fit with Eq. (7) yields a saturation illumination power of 680 μW corresponding to an average focal intensity of $\sim 500 \text{ kW cm}^{-2}$ in agreement with previous results [33], and EGFP has a similar saturation intensity [34]. Since all FCS experiments were carried out well below 200 μW or 150 kW cm^{-2} whereas all images were taken at 400-500 μW , the saturation effect on the PSF should be negligible for

FCS and noticeable for RICS and msICS. We could confirm the influence of saturation with FCS measurements of the Alexa488 solution where the diffusion correlation time and the derived focal radius increased with increasing illumination power, see Fig. 2a.

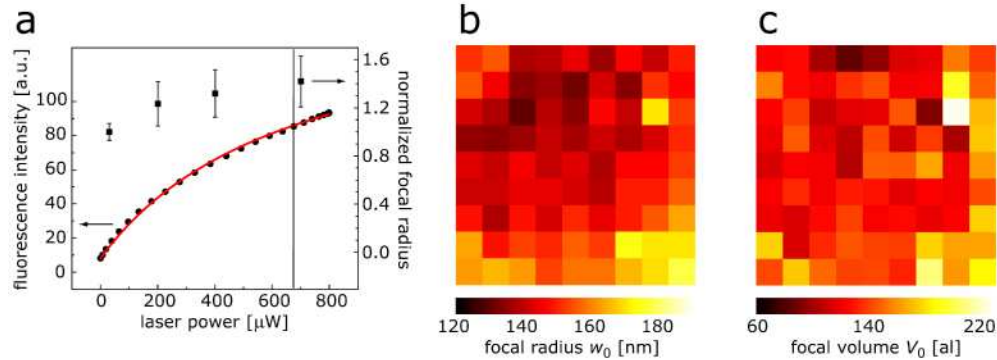


Fig. 2. Characterization of the PSF. (a) Mean fluorescence intensity of Alexa488 taken from confocal images (circles, left axis) and the fit of Eq. (7) (red line) as well as the focal radius normalized to the value determined at 30 μW (squares, right axis) as a function of incident laser intensity. The vertical line marks the saturation power. (b) Map of the focal radius w_0 and (c) of the focal volume V_0 as determined with FCS of Alexa488 in solution on a 9×9 array of points covering an area of $243 \times 243 \mu\text{m}^2$. The variations are very small within the central $135 \times 135 \mu\text{m}^2$ area where the experiments were carried out.

To ensure that the focal volume of the laser beam is sufficiently homogenous throughout the field of view (FOV) and does not affect the resulting diffusion coefficient, we generated a map of 9×9 FCS point measurements of 20 nM Alexa 488 (5x60 s each) yielding the characteristic diffusion correlation time τ_{diff} and structure parameter κ . Using $D_{\text{Alexa}, 20^\circ\text{C}} = 210 \mu\text{m}^2 \text{s}^{-1}$ [35], distribution maps of the lateral focal radius w_0 in μm and the focal volume V_0 in μm^3 or fl, respectively, were obtained, see Fig. 2b, c. Average values for w_0 and V_0 are $0.140 \pm 0.003 \mu\text{m}$ and $0.126 \pm 0.017 \text{ fl}$, respectively, for the central 3×3 array of $81 \times 81 \mu\text{m}^2$ and $0.141 \pm 0.005 \mu\text{m}$ and $0.125 \pm 0.016 \text{ fl}$, respectively, for the central 5×5 array of $135 \times 135 \mu\text{m}^2$. Thus in these areas, to which the experiments were restricted, the focal volume can be assumed constant.

4.2 RICS experiments

RICS experiments were done to verify the guidelines given in Eq. (4) and by Digman et al. [17]. The correlation curves were plotted and fitted for at least the first 30 pixel shifts along the line in x direction, always without $\xi = 0$ because of the strong autocorrelation of the shot noise. Pixel shifts in y direction were not used because the line times are >1 ms and thus much larger than τ_{diff} . Experiments performed with dyes in solution showed that the fitted diffusion coefficient showed some variation with the used scanning velocity. For the same scanning velocity higher sampling yielded better results.

Figure 3 shows an example of a RICS experiment performed in an EGFP-expressing HeLa cell where a 50×50 pixel, $1.5 \times 1.5 \mu\text{m}^2$ ROI was chosen in the nucleolus with varying scanning velocities (pixel dwell times) and a constant pixel shift of 30 nm. In the cytoplasm the apparent diffusion coefficient of EGFP is expected to be $\sim 23 \mu\text{m}^2 \text{s}^{-1}$ [36–38]. Due to obstacles presented by the nuclear structure, especially in the nucleolus [31, 39] the resulting apparent diffusion coefficient should be smaller than in the rest of the cell. Although this obstruction effect could be described in principle with anomalous diffusion, we obtained an apparently reduced diffusion coefficient because the signal-to-noise ratio of our measurements did not allow to distinguish anomalous from free diffusion. We chose scanning frequencies resulting in pixel dwell times between 9.4 and 37.3 μs and scanning velocities between 805 and 3198 $\mu\text{m s}^{-1}$, respectively, complying with the recommended range and covering the value of 980 $\mu\text{m s}^{-1}$ determined with Eq. (4). Table 1 shows that we could obtain

reasonable fit results for every pixel dwell time. However, each data point featured a rather large error most likely

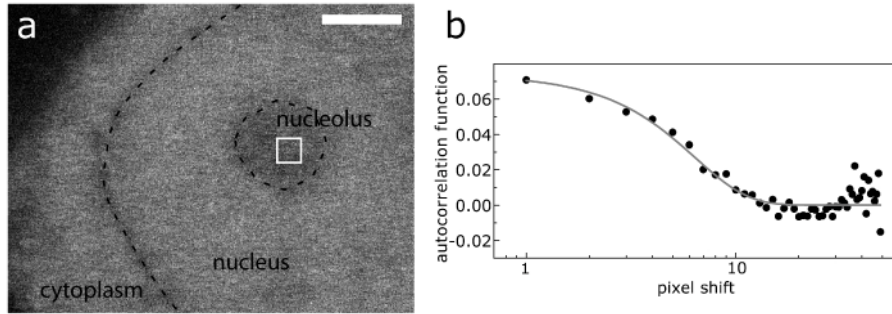


Fig. 3. RICS in a living cell. (a) Detail of a confocal image of a HeLa cell expressing EGFP with a ROI in the nucleolus (white square; 50×50 pixels, $1.5 \times 1.5 \mu\text{m}^2$) used for RICS analysis (scale bar $5 \mu\text{m}$): (b) autocorrelation function averaged over 7 images acquired at 35 Hz scanning frequency (circles) and fit (line) of Eq. (2) yielding a diffusion coefficient of $23 \mu\text{m}^2 \text{s}^{-1}$.

Table 1. Diffusion coefficients D from RICS and FCS experiments in EGFP-expressing HeLa cells

f_{scan} [Hz] ^a	τ_p [μs] ^b	v [$\mu\text{m s}^{-1}$] ^c	D [$\mu\text{m}^2 \text{s}^{-1}$]
35	9.4	3198	$23 + 39/- 21$
20	17.8	1690	$27 + 39/- 27$
15	24.3	1237	$31 + 38/- 29$
10	37.3	805	$16 + 37/- 15$
global/average			24.4 ± 6.7
point FCS ^d			21.9 ± 4.7

^a scanning frequency

^b pixel dwell time

^c scanning velocity

^d apparent diffusion coefficient using τ_{diff} from an anomalous diffusion fit but the equation for free diffusion

because the ROI was very small. This could be reduced significantly by averaging as well as global analysis over different scanning velocities which led us to the msICS approach where a systematic “scan” of pixel dwell times is employed. It should be noted that both RICS and msICS experiments are less sensitive to saturation effects than FCS because the pixel shift is independent of the optical resolution and both the diffusion coefficient D and the focal radius w_0 are independent fit parameters. Indeed w_0 obtained from fits to all RICS and msICS data was ~ 200 nm, i.e. as large as determined with FCS at the same excitation intensity and $\sim 40\%$ larger than at lower intensities as typically used for FCS experiments (~ 140 nm). This is in good agreement with the saturation-induced intensity dependence of the focal radius as shown in Fig. 2a.

4.3 msICS experiments with fluorophores in solution

To evaluate the msICS approach we used Alexa488 in aqueous solution (20 nM). The ROI was set to 200×200 pixels ($6 \times 6 \mu\text{m}^2$) and the fits were carried out either separately for different pixel shifts ($\xi = 1$ and $\xi = 2$, see Fig. 4a) or globally ($\xi = 1, 2$ and $\xi = 1 \dots 10$, see Fig. 4b). As Table 2 shows, the resulting diffusion coefficients were in good agreement with our expectations and conventional point FCS measurements, see Fig. 4c. Especially the $\xi = 1$ and the $\xi = 2$ correlation functions strongly resembled the point FCS correlation function, featured a comparable signal-to-noise ratio and allowed a good fit. Like in other multifocal FCS implementations, the result is less dependent on aberrations of the PSF.

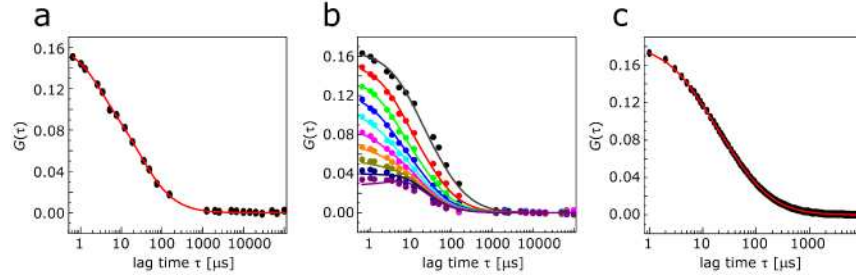


Fig. 4. msICS in solution. (a) msICS, $\xi = 2$, of Alexa488 (20 nM) from a ROI of 200×200 pixels and $6 \times 6 \mu\text{m}^2$ (circles) and fit (line) with Eq. (2). (b) msICS, $\xi = 1 \dots 10$ (circles, decreasing amplitude with increasing ξ), of the same sample and ROI with global fit (lines). (c) Point FCS of the same sample (circles) and fit (line) with Eq. (7). For fit results see Table 2.

Table 2. Diffusion coefficients D from msICS experiments of Alexa488

pixel shift ξ	$D [\mu\text{m}^2 \text{s}^{-1}]$
1	245 ± 8
2	210 ± 13
1, 2 (global)	220 ± 12
1...10 (global)	235 ± 12
0 (FCS)	210 ± 21

4.4 msICS experiments with HeLa cells expressing EGFP

We tested the applicability of msICS *in vivo* with HeLa cells expressing EGFP. Figure 5 shows the msICS curves for the pixel shifts $\xi = 1 \dots 10$ acquired in a nucleolus and evaluated for a single ROI of 100×100 pixels ($3 \times 3 \mu\text{m}^2$). It demonstrates how this approach extends the RICS concept: in one dimension (pointing to the right), it shows the msICS curves to given pixel shifts whereas in the other dimension, it represents the RICS correlation functions to given scanning frequencies with the pixel shift contribution at lag times below a lag time of $\sim 200 \mu\text{s}$ and the line shift contribution above. From a global fit of Eq. (2) to the data, an apparent diffusion coefficient of $10.2 \pm 1.7 \mu\text{m}^2 \text{s}^{-1}$ was obtained in agreement with point FCS measurements we performed in these cells and with previous studies based on FCS [31, 37, 39]. After reducing the ROI size at the same position to 50×50 pixels ($1.5 \times 1.5 \mu\text{m}^2$) the fit produced a rather comparable diffusion coefficient of $12.2 \pm 5.1 \mu\text{m}^2 \text{s}^{-1}$, albeit with a larger error. Thus such a ROI provides usable data with spatial resolution enabling to map diffusion coefficients with $\sim 1 \mu\text{m}$ sampling. For even smaller ROIs (e.g. 30×30 pixels) the data became too noisy to be evaluated.

To actually allow to fit the data, a correction for slowly mobile or immobile structures had to be applied as described above using various sizes d of the moving average filter, see Eq. (6). For 50×50 pixel ROIs a useful size was in the range of 31-81 pixels, i.e. large enough to leave the diffusional fluctuations unaffected but small enough to actually remove slow or static fluctuations, so that we applied $d = 51$ to all subsequent experiments.

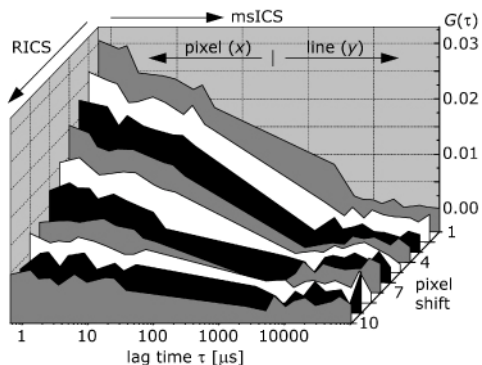


Fig. 5. Two-dimensional graph of the autocorrelation functions of data acquired in the nucleolus of a HeLa cell expressing EGFP (ROI: 100×100 pixels, $3 \times 3 \mu\text{m}^2$), plotted over the pixel shift ξ (RICS curves, fixed τ_p) and the pixel dwell time τ_p /line time τ_l (msICS curves, fixed ξ).

4.5 Map of diffusion coefficients

As shown above, msICS should allow to generate maps of the mobility of EGFP in HeLa cells. Figure 6a shows an example of a HeLa cell expressing EGFP, an area of which was divided into 13×15 ROIs (each 50×50 pixels, $1.5 \times 1.5 \mu\text{m}^2$) covering $10.5 \times 12.0 \mu\text{m}^2$ at two-fold oversampling and including different cellular compartments represented by msICS curves from a nucleolus, the nucleoplasm and the cytoplasm (Fig. 6b). An evaluation as described in the previous section yields a diffusion coefficient for every ROI that can be used for a two-dimensional map, see Fig. 6c for a contour plot representation. It should be noted that there are always data sets that are too noisy to be analyzed. Variations in the mobility of the EGFP molecules represented here by the apparent diffusion coefficient are mainly due to different degrees of obstruction of the diffusion process caused by subcellular structures such as chromatin and associated complexes of different densities in the nucleus and the nucleolus or the endoplasmic reticulum (ER) in the cytoplasm [31, 39, 40]. From 6 experiments, we could distinguish the apparent diffusion coefficient of $20.4 \pm 2.4 \mu\text{m}^2 \text{s}^{-1}$ in the nucleoplasm from $9.5 \pm 1.4 \mu\text{m}^2 \text{s}^{-1}$ in the nucleoli.

5. Conclusion

Multiple scan speed intensity correlation spectroscopy (msICS) is a useful tool to measure and map the diffusion of molecules with spatial resolution in living cells. It extends the concept of RICS and benefits likewise from the fact that widely accessible CLSM equipment can be used. In msICS data, the spatial and the temporal information inscribed into a CLSM image are uncoupled but remain subject to a spatio-temporal correlation analysis. In this way, it covers a broad time regime for the processes of interest, for which a priori knowledge is not required, and provides correlation data that are comparable to conventional FCS experiments. It can be applied to subregions of confocal images in a rasterized way so that maps of correlation functions and of the derived parameters can be created.

We could show that spatio-temporal correlation methods are less sensitive to saturation effects on the PSF. We applied RICS to fluorophores in solution and to HeLa cells expressing EGFP and could see that the statistical relevance of the data increased significantly when acquiring images at several scanning velocities (albeit at the cost of the total acquisition time) and employing global fits, resulting in the msICS concept. We devised a strategy to correct for photobleaching and for slow or immobile structures. This allowed us to use msICS to measure the diffusion of fluorophores in solution with a data quality similar to FCS. We also obtained apparent diffusion coefficients of EGFP in HeLa cells in the range of 10 - $20 \mu\text{m}^2 \text{s}^{-1}$ in good

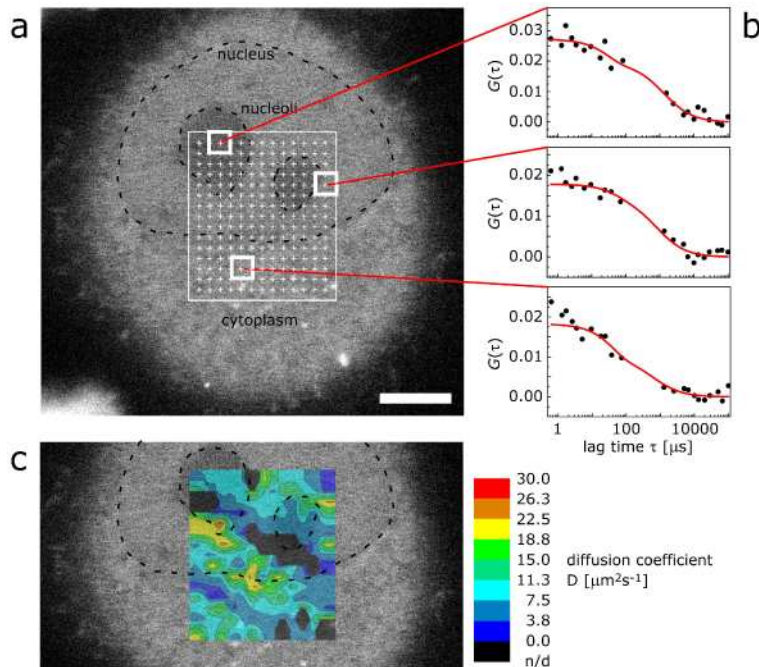


Fig. 6. Map of msICS-derived diffusion coefficients of a HeLa cell expressing EGFP. (a) A $10.5 \times 12.0 \mu\text{m}^2$ area covering parts of the cytoplasm, the nucleus and the nucleoli was sampled with 13×15 ROIs (50×50 pixels, $1.5 \times 1.5 \mu\text{m}^2$, white squares) that were centered around the white crosses corresponding to two-fold oversampling and used for msICS analysis (scale bar $5 \mu\text{m}$). (b) autocorrelation curves ($\xi = 1$, circles) and fits (red lines) of Eq. (2) acquired at positions in a nucleolus, the nucleus and the cytoplasm yielding diffusion coefficients of 8.1 , 7.6 , and $5.6 \mu\text{m}^2 \text{s}^{-1}$, respectively. (c) Resulting contour map of diffusion coefficients (black for areas where the correlation analysis failed – n/d, not determined).

agreement with previous results. With a generated map of apparent diffusion coefficients some structural information could be correlated with molecular mobilities with a resolution in the order of $1 \mu\text{m}$ confirming that especially in the nucleolus of HeLa cells in interphase, the density of the genetic material strongly obstructs the molecular diffusion.

Alternative approaches implement fully sequential acquisition of point FCS measurements by scanning the stage or the beam [39, 41] with comparably high temporal resolution but either limited range of accessible lag times or comparably long total measurement time, or they employ multifocal camera-based setups for parallelized acquisition [42–44] where the measurement time is significantly reduced, however at the cost of time resolution. Our approach bridges the gap between dedicated custom-designed setups and the conventional CLSM with the corresponding raster-scanning scheme as used for msICS ideally in combination with photon-counting detectors. It makes msICS a promising tool to measure and map even more complex diffusion processes with data similar to conventional FCS.

Acknowledgements

This work was supported by the EpiSys project within the BMBF SysTec program. We would like to thank Jessica Kehrer (EMBL) for help with the cell culture, the Advanced Light Microscopy Facility of EMBL for their support, Rolf Borlinghaus and Lioba Kuschel (Leica Microsystems) for fruitful discussions and for providing some of the microscopy equipment.